Self-Assembled Nanoparticles from a Block Polyelectrolyte in Aqueous Media: Structural Characterization by SANS

Aristeidis Papagiannopoulos,*,† Maria Karayianni,† Grigoris Mountrichas,†,‡ Stergios Pispas,*,† and Aurel Radulescu§

Theoretical and Physical Chemistry Institute, National Hellenic Research Foundation, 48 Vassileos Constantinou Avenue, 11635 Athens, Greece, Institut de Chimie de la Matière Condensée de Bordeaux (ICMCB), Centre National de la Recherche Scientifique (CNRS), 87 Avenue du Docteur Albert Schweitzer, 33608 Pessac Cedex, France, and Institut für Festkörperforschung, Forschungszentrum Jülich GmbH, Jülich Centre for Neutron Science at FRM II, Lichtenbergstrasse 1, 85747 Garching, Germany

Received: February 2, 2010; Revised Manuscript Received: April 15, 2010

We present a small angle neutron scattering (SANS) study of polystyrene-*b*-sodium (sulfamate/carboxylate) isoprene (PS-PSCI) nanoparticles in aqueous media. The SANS experiments are complemented by static and dynamic light scattering measurements. A detailed analysis of the scattering form factor obtained by SANS for the self-assembled block polyelectrolyte spherical nanoparticles implies a two-region power-law model for the radial volume fraction profiles. The theoretically predicted scaling of the osmotic brush regime $\phi(r) \sim r^{-2}$ for the inner region and the osmotic annealing brush regime $\phi(r) \sim r^{-8/3}$ for the outer region are in agreement with our experimental findings. A concentrated shell of PSCI polyelectrolyte chains collapsed on the polystyrene core is needed in the form factor analysis so that the aggregation number of the nanoparticles is self-consistent. The self-assembled nanoparticles are found to be kinetically frozen i.e. their aggregation number is not sensitive to the solution conditions and is defined by the preparation protocol. The size of the spherical nanoparticles tends to decrease upon the addition of salt and the drop of pH.

Introduction

Self-assembled nanoparticles formed by amphiphilic block copolymers and block polyelectrolytes find applications in bionanotechnology as functional nanobiomaterials, including drug nanocarriers.[1] The study of such systems attracts considerable attention for basic understanding of the behavior and structure formation. Block polyelectrolytes with one hydrophobic and one polyelectrolyte block form micellar particles in water.[2] Polyelectrolyte brushes,[3] like the ones found in the corona of spherical block polyelectrolyte micelles, have a range of diverse properties because of their response to solution conditions,[4] i.e. ionic strength and pH, compared to uncharged systems. Long range nature of electrostatic interactions, dependence of the degree of dissociation on pH for weak polyelectrolytes,[5] charge condensation, counterion osmotic pressure and polymer backbone flexibility and solubility are parameters that complicate the understanding of morphology, dynamic behavior and interactions in these systems.

At low ionic strength and high density of polymer chains on a surface grafted with polyelectrolyte molecules the counterion osmotic pressure balances the polymer elasticity and the chains are fully stretched.[6] This is the osmotic brush regime.[7] The osmotic brush retains its size independently of salt content until the solution ionic strength exceeds the ion concentration inside the brush. Then the electrostatic interactions are screened and the size of the brush reduces as the ionic strength increases. At high salt contents the electrostatic interactions are short-ranged and the properties of the brush are reminiscent of those of uncharged brushes either in planar[8] or in spherical geometries.[9] In the case of weak polyelectrolytes[5] the number of charges on the polyelectrolyte chains depend on the pH of the solution and the size of the brush is not a monotonous function of ionic strength because of the interplay between counterions and salt ions.

We have studied the structure and dynamics of polyelectrolytes in comb geometry in the past.[10] SANS experiments were consistent with cylindrical polyelectrolyte brushes[11] in solution. They are potential candidates for arthritic condition replacements, viscosity modifiers and also model systems for biological counterparts.[12]

Small angle scattering techniques are powerful noninvasive methods for in situ structural analysis of synthetic, biological and hybrid systems. Small angle neutron scattering (SANS) utilizes the contrast difference between hydrogenated and deuterated parts of a polymer solution.[13] There are numerous treatments that can extract information about the size, shape and segment distribution of colloidal particles and polymeric nanostructures, along with the interactions and aggregation behavior.[14] Structural information in solution is important for understanding the dynamics, stability and possible applications of such systems.

A complex structural morphology is expected for our nanoparticles, and a detailed SANS investigation is very crucial for their experimental testing in protein complexation[15] and their potential application as drug nanocarriers. In this paper we present SANS data from nanoparticles formed by the self-assembly of diblock polyelectrolyte polystyrene-*b*-sodium (sulfamate/carboxylate) isoprene in aqueous solutions. The water-soluble block contains hydrophobic isoprene groups, pH dependent chargeable groups (COO^-H^+) and strongly charged groups ($SO_3^-Na^+$), Figure 1. The conformation of the spherical

* To whom correspondence should be addressed, e-mail: aristeidis.papagiannopoulos@gmail.com; pispas@eie.gr.
† National Hellenic Research Foundation.
‡ ICMCB, CNRS.
§ Forschungszentrum Jülich GmbH.

10.1021/jp1009912 © 2010 American Chemical Society
Published on Web 05/18/2010

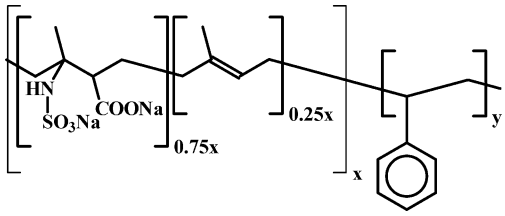

Figure 1. Chemical structure of PS-PSCI diblock polyelectrolyte. The degrees of polymerization are $n \approx 96$, $m \approx 1136$, and the degree of functionalization is 75% (molar).

polyelectrolyte brushes is extracted under different solution conditions. Static and dynamic light scattering is also employed in order to complement the SANS results.

Materials and Methods

Sample Preparation. The diblock copolymer polystyrene-*b*-sodium (sulfamate/carboxylate) isoprene was synthesized by a combination of anionic polymerization and post polymerization functionalization reactions as described in detail elsewhere.[16,17] The copolymer utilized in this study has a weight average molecular weight $M_w = 244{,}500$, and the weight fraction of PS and PSCI blocks is 4.1% and 95.9% respectively (Figure 1). The PSCI block consists of isoprene units that are randomly functionalized with hydrophilic sulfamate and carboxylate groups at a proportion of 75%. It is an intrinsically flexible hydrophobic polymer that dissolves in water because of the dissociating units contained in its functionalized segments. In aqueous media PSCI has one strongly charged group i.e. SO_3^- (with Na^+ as a counterion) and a weak acidic group COO^- which is neutralized by H^+ at pH below 4.2[18] (Figure 1). The number of monomers is 96 on the PS block and 1134 on the PSCI block.

For the preparation of the nanoparticles 30 mg of PS-PSCI is stirred for 1 h in 10 mL of tetrahydrofuran (THF, from Fluka, UV spectroscopy grade) at 60 °C. Subsequently, 30 mL of distilled water or D_2O (for light scattering or SANS measurements respectively) was added dropwise under vigorous stirring. THF was then removed by evaporation at 65 °C under stirring. The final concentration of PS-PISC nanoparticles in the resulting aqueous solutions was 1 mg/mL. Lower concentrations were prepared by dissolution with the desired amount of water or D_2O. The pH was set by adding NaOH or HCl (NaOD or DCl in D_2O in order to minimize the incoherent scattering in SANS). The contribution of the added acid or base to the ionic strength was about 10^{-4} M. The added salt used was NaCl. Samples for SANS or light scattering were filtered with 0.45 μm PVDF membrane filters in order to remove any large aggregates or dust particles.

Small Angle Neutron Scattering. Small angle neutron scattering (SANS) experiments were performed on the KWS-2 high intensity/wide-q small angle neutron diffractometer, at the research reactor FRM II (Jülich Centre for Neutron Science). The nominal scattering vector (q) range is 0.002 to 0.2 $Å^{-1}$ (real space length scales ~1000 to 10 Å). This range was covered by three separate detection/neutron wavelength configurations. The high q range was measured at 2 m detection length with a 4.5 Å wavelength, and the intermediate and low q ranges were measured at 8 m detection length with 4.5 Å and 19 Å neutron wavelengths respectively.

SANS Data Analysis. The collected 2-D raw data was corrected for the scattering from the empty cell, the solvent, and the electronic and background noise, and finally the scattered intensity was calibrated to absolute scale using lupolen and plexiglass as a standard. After azimuthal integration of the 2-D data the scattered intensity $I(q)$ was obtained as a function of the scattering vector (q). The last depends on the neutron wavelength (λ) and scattering angle (θ) as $q = 4\pi/\lambda \sin\theta$.

The chemical composition of the PS-PSCI diblock copolymer suggests the formation of spherical nanoparticles in aqueous solution. The diblock copolymer chains are expected to self-assemble with their short PS blocks forming a hydrophobic core surrounded by a polyelectrolyte shell of the long PSCI blocks.

Spherically symmetric models were employed to describe the conformation of the system. The neutron scattering length density ρ is a function only of the distance r from the particle's center, i.e. $\rho \equiv \rho(r)$. The scattered intensity, intraparticle form factor, from such particles in solution can be calculated, neglecting intermicellar correlations and/or cluster formation, by[13]

$$I^{th}(q) = N_p\left\{4\pi \int_0^\infty (\rho(r) - \rho_{solvent}) r^2 \frac{\sin qr}{qr}\, dr\right\}^2 \quad (1)$$

The number of particles per unit volume is N_p.

The scattering length density is related to the volume fraction profile of the polymer in solution through

$$\rho(r) = \varphi(r)\rho_{polymer} + (1 - \varphi(r))\rho_{solvent} \quad (2)$$

In our case $\rho_{solvent} = 6.4 \times 10^{10} cm^{-2}$ is the scattering length density of D_2O and $\rho_{polymer}$ the scattering length density of PS or PSCI ($\rho_{PS} = 1.41 \times 10^{10} cm^{-2}$, $\rho_{PSCI} = 1.17 \times 10^{10} cm^{-2}$).

We have taken the instrumental smearing[19] into account by convoluting the theoretical $I^{th}(q)$ of eq 1 with a Gaussian function for the statistical distribution of the uncertainty in q, i.e.

$$I(q) = \frac{1}{\sqrt{2\pi}\Delta q(q)} \int_{-\infty}^{+\infty} e^{-\left(\frac{q'-q}{\sqrt{2}\Delta q(q)}\right)^2} I^{th}(q')\, dq' \quad (3)$$

The standard deviation $\Delta q(q)$ is calculated from the contributions of the instrument's resolution $\Delta\lambda/\lambda = 0.2$, the beam-stop shadowing effects and the apertures configuration.

The scope of the analysis is to fit optimal models of $\varphi(r)$ to the experimental curves by the use of eq 3. The integration of eqs 1 and 3 was done numerically by Gaussian quadrature and Simpson's rule respectively. The minimization of $\chi^2 = \sum_{i=1}^{N}\{[I^{exp}(q_i) - I^{mod}(q_i)]/\sigma_i\}^2$ was performed with the nonlinear SIMPLEX method.[11] N is the number of experimentally obtained data points, I^{exp} and I^{mod} are the experimental and the model calculated values and σ_i is the uncertainty of I^{exp}. The reduced value of χ^2, $\chi_r^2 = \chi^2/(N - M)$ (M is the number of fitting parameters), is used to describe the quality of the fits, and a value near unity is the optimal one.[20]

Light Scattering. Light scattering measurements were performed on an ALV/CGS-3 compact goniometer system (ALVGmbH, Germany), equipped with a ALV-5000/EPP multi tau digital correlator and a He−Ne laser operating at the wavelength of 632.8 nm. Field autocorrelation functions were obtained at a series of angles in the range 20−150° for dynamic light scattering. In static light scattering the Rayleigh ratio for block copolymer solutions was calculated with respect to a toluene standard. Samples were loaded into standard 1 cm

diameter Helma quartz cells. Static light scattering (SLS) measurements were performed at a series of angles in the range 20−150°.

Static light scattering data were treated by the Zimm plot:

$$\frac{Kc}{R(q,c)} = \frac{1}{M_w P(q)} + 2A_2 c \tag{4}$$

where M_w is the weight-averaged molar mass and A_2 the "light-scattering-averaged" osmotic second virial coefficient of the polymer in solution. $R(q,c)$ is the corrected Rayleigh ratio. $P(q)$ is the particle form factor $P(q) = 1 - (1/3)\langle S^2\rangle_z q^2$ and $\langle S^2\rangle_z$ is the squared z-averaged radius of gyration and K the contrast factor.[17]

In the dynamic light scattering (DLS) the field autocorrelation functions $g^{(2)}(t)$ are collected at different scattering angles and analyzed by the CONTIN algorithm. The characteristic relaxation rate $\Gamma(q)$ is taken from the position of the maximum of the distribution function of relaxation times ($\Gamma(q) = 1/\tau(q)$). In the case of diffusive modes there is a linear relation between $\Gamma(q)$ and q^2, i.e. $\Gamma(q) = Dq^2$, and the diffusion coefficient D is obtained. The hydrodynamic radius, R_h, is extracted from the Stokes−Einstein equation

$$R_h = \frac{k_B T}{6\pi\eta D} \tag{5}$$

where η is the viscosity of the solvent, k_B is the Boltzmann constant and T is the temperature.

Results

Two-Region Power-Law Model for the Corona Conformation. Core−corona structures are often used to model diblock polyelectrolyte micelles in solution.[21,22] A power-law function for the corona density profile derived for star polymers has been shown to be efficient for polymeric micelles.[23] We have tested single-region and double-region power-law volume fraction profiles as shown in eq 6 where we assume a core of solid PS surrounded by a corona of PSCI chains immersed in water.

$$\varphi(r) = \begin{cases} 1 & \text{for } 0 \le r < R_c \\ \varphi_1\left(\dfrac{r}{R_c}\right)^{-a} & \text{for } R_c \le r < R_{int} \\ \varphi_2\left(\dfrac{r}{R_{int}}\right)^{-b} & \text{for } R_{int} \le r < R_M \end{cases} \tag{6}$$

where R_c is the radius of the core, and the inner power-law region extends from R_c to R_{int} and the outer one from R_{int} to R_M. Furthermore φ_1 and φ_2 are the initial volume fractions of each power-law region. The model of eq 6 is reduced to a single-power law model when $\varphi_2 = 0$. Figure 2 shows SANS data after subtraction of the scattering from pure solvent from 1 mg/mL solution of nanoparticles at pH 7 with 0.5 M added salt. The background scattering (I_{inc}) is mainly due to the incoherent scattering of the hydrogenated parts of the copolymers and is incorporated to the calculated $I(q)$ by adding a constant factor. A 2-region profile results in $\chi_r^2 \approx 1.4$ compared to a 1-region model with $\chi_r^2 \approx 4.6$. A second corona layer provides a better fit to the data both at low q because it inserts a larger length scale (R_M) and at intermediate q (0.008 − 0.02 Å^{-1}) by removing the artificial oscillation around the experimental data which is

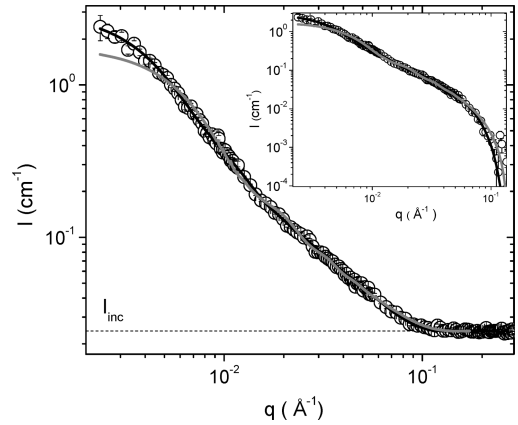

Figure 2. SANS scattered intensity from 1 mg/mL PS-PSCI nanoparticles at pH 7 with 0.5 M NaCl. The gray line is the best fit with a one-region core−corona model and the black line the best fit with a two-region model. In the inset the same set of data is shown after subtraction of the constant incoherent background I_{inc} to pronounce the shape of the high-q regime.

observed for the single-region model. At high q (i.e., short length scales) the scattering is dominated by the core structure and both models (1- and 2-region) fit efficiently (Figure 2, inset). Therefore we select the 2-region power-law profile for the SANS analysis of the corona. Finally we do not include any polydispersity effects since it does not improve the fits and additionally it tends to smooth the curvature of the fitting curves in the range of 0.01−0.02 Å^{-1}.

Detailed Profile Analysis. The aggregation number (N_{agg}) of the nanoparticles (i.e., number of diblock polyelectrolyte chains per nanoparticle) can be deduced from the well-defined size of the PS-core from our SANS data. Assuming that the core consists only of PS then the aggregation number is calculated with the use of the density (d_{PS}) of the solid PS:

$$N_{agg}^{core} = \frac{4}{3}\pi {R_c}^3 d_{PS} \frac{N_A}{M_{PS\text{-}BLOCK}} \tag{7}$$

where N_A is Avogadro's number. Since the PSCI chains are covalently bonded to the PS chains, the aggregation number can be also expressed through the amount of the PSCI block in the corona:

$$N_{agg}^{corona} = d_{PSCI} \frac{N_A}{M_{PSCI\text{-}BLOCK}} 4\pi \int_{R_c}^{R_M} r^2 \varphi(r)\, dr \tag{8}$$

The radius of the core is about 3.2 nm and is fairly constant in all of our SANS data sets because it is determined by the high-q region, which is the same within experimental error for all of them. The core size of 3.2 nm corresponds to $N_{agg}^{core} \approx 8$. From the corona volume fraction profile we find $N_{agg}^{corona} \approx 3$. If we incorporate the constraint for $N_{agg}^{core} = N_{agg}^{corona}$ in the fitting algorithm, we fail to fit the experimental data because this restriction tends to decrease the size of the core and/or increase the size and volume fraction of the corona. Consequently the calculated $I(q)$ changes shape. This shows that the scattering length density profile $\rho(r)$ that defines $I(q)$ (eq 2) is not amenable to significant changes from the initially fitted profile. One way to keep $\rho(r)$ virtually unchanged and at the same time satisfy $N_{agg}^{core} = N_{agg}^{corona}$ is to assume that the core region contains both PS and PSCI blocks. This leads us to conclude that the part of

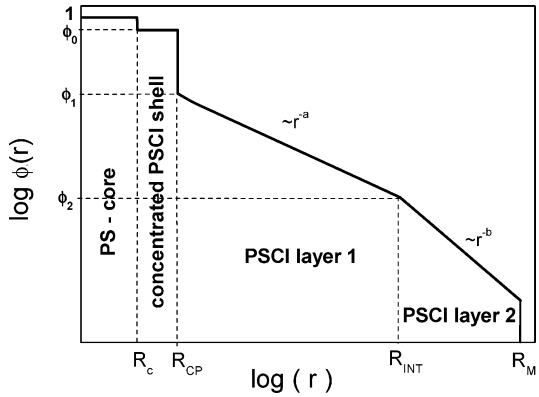

Figure 3. Model volume fraction profile as a function of the distance from the center of the nanoparticle. The core consists of PS and is surrounded by a dense PSCI shell. The corona of dissolved PSCI chains is described by two regions of different power-law behavior.

the nanoparticle which is responsible for the high-q scattering contains a concentrated spherical shell of PSCI which surrounds the PS-core and is nearly contrast matched to the PS-core. Introducing this PSCI layer with constant volume fraction next to the core and incorporating the constraint $N_{agg}^{core} = N_{agg}^{corona}$ gives even better fits to our data (in terms of χ_r^2) and also defines the aggregation number of the nanoparticle consistently. This layer, defined by the radii R_c and R_{CP} (eq 9), corresponds to PSCI chains collapsed on the hydrophobic PS-core.

The model we used to fit all of the SANS patterns in this study is described in eq 9 and is depicted in Figure 3.

$$\varphi(r) = \begin{cases} 1 & \text{for } 0 \le r < R_c \\ \varphi_0 & \text{for } R_c \le r < R_{CP} \\ \varphi_1\left(\dfrac{r}{R_c}\right)^{-a} & \text{for } R_c \le r < R_{int} \\ \varphi_2\left(\dfrac{r}{R_{int}}\right)^{-b} & \text{for } R_{int} \le r < R_M \end{cases} \quad (9)$$

The profile of eq 9 implies optimizing the values of 7 parameters, i.e. R_c, R_{CP}, R_{int}, R_M, ϕ_1, a and b. The value of ϕ_0 is fixed so that the constraint $N_{agg}^{core} = N_{agg}^{corona}$ is fulfilled, and ϕ_2 is set so that the volume fraction profile is continuous at R_{int}. When ϕ_2 is a free parameter, the resulting profiles are either continuous or nearly continuous, so the choice to set ϕ_2 does not bias the fitting and reduces the number of fitting parameters.

In Figure 4 the scattering profiles and the fitting curves for samples in different ionic strengths are plotted, and in Figure 5 the resulting curves at pH 3 and pH 9 values are shown. The value of R_c falls into the same range for all data sets (table 1) within uncertainty, and this shows that the PS-core and therefore the aggregation number N_{agg} remain unaltered under different solution conditions. R_{CP} is also fairly unaffected by the solution conditions and is common for all data sets. Table 1 also contains the values of the exponents a and b which also remain unaltered within experimental error. Table 2 contains the rest three of the resulting optimized parameters (R_{int}, R_M, ϕ_1), as well as the volume fraction ϕ_0 in the concentrated shell and the radius of gyration of the particles. The radius of gyration is obtained from the SANS results by integrating the volume fraction profile as in eq 10.

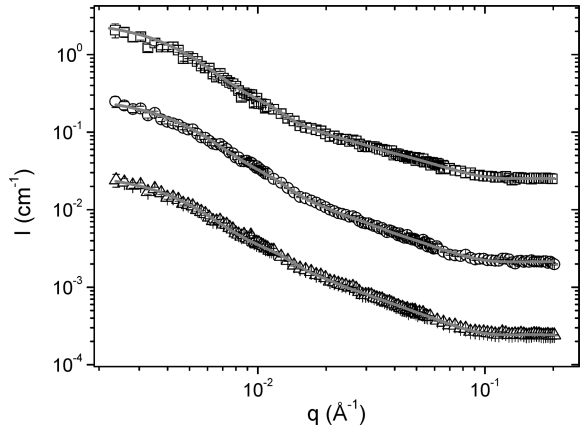

Figure 4. Scattered intensity fitted (gray lines) by the two-region power law model (Figure 3) of 1 mg/mL PS-PSCI nanoparticles at pH 7 with no added salt (squares), 0.1 M added NaCl (circles) and 0.5 M added NaCl (triangles). Data sets of 0.1 and 0.5 M are divided by 10 and 100 respectively for clarity.

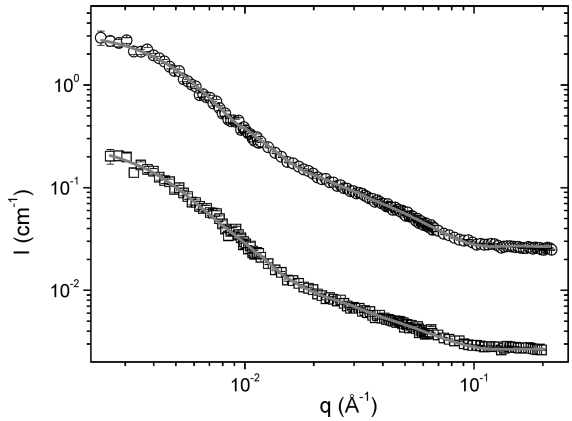

Figure 5. Scattered intensity fitted (gray lines) by the two-region power law model (Figure 3) of 1 mg/mL PS-PSCI nanoparticles with no added salt at pH 3 (circles) and pH 9 (squares). The data set of pH 9 is divided by 10 for clarity.

TABLE 1: Parameters Extracted from SANS Which Are Common for All the Data Sets at Different Solution Conditions

R_c (nm)	R_{CP} (nm)	a	b	N_{agg}
2.50 ± 0.05	3.6 ± 0.1	1.8 ± 0.2	3.0 ± 0.5	4.1 ± 0.3

$$R_g^2 = \frac{\int_0^{R_M} r^4 \varphi(r)\, dr}{\int_0^{R_M} r^2 \varphi(r)\, dr} \quad (10)$$

We have tested the influence of concentration on the scattering curves (Figure 6). The scattering from colloidal particles is normally expressed as

$$I(q) = N_p P(q)\, S(q) \quad (11)$$

In our treatment we have neglected the interparticle correlations which are expressed by the structure factor $S(q)$ which is expected to change the shape of the scattering curves systematically as the concentration changes.[24] This is because the characteristic distance between particles is connected to their concentration. As shown in Figure 6 there is no systematic difference between the curves from 3 concentrations. The curves are normalized by the corresponding nominal concentration to

TABLE 2: Parameters Extracted from SANS for PS-PSCI Diblock Polyelectrolyte Nanoparticles at Different Solution Conditions

	R_{int} (nm)	R_M (nm)	ϕ_0	ϕ_1	R_g (nm)	R_g (nm) (SLS)	R_h (nm) (DLS)	N_{agg} (SLS)
pH 7, no added salt	28 ± 2	82 ± 5	0.70 ± 0.10	0.090 ± 0.01	39 ± 4	43 ± 5	77 ± 7	3 ± 1
pH 7, 0.1 M NaCl	27 ± 2	78 ± 5	0.67 ± 0.10	0.13 ± 0.01	36 ± 4	49 ± 5	56 ± 6	6 ± 1
pH 7, 0.5 M NaCl	24 ± 2	75 ± 5	0.75 ± 0.10	0.13 ± 0.01	36 ± 4	53 ± 5	60 ± 6	8 ± 1
pH 3, no added salt	28 ± 2	71 ± 5	0.92 ± 0.10	0.10 ± 0.01	34 ± 4	53 ± 5	53 ± 5	6 ± 1
pH 9, no added salt	28 ± 2	86 ± 5	0.80 ± 0.10	0.100 ± 0.01	39 ± 4	45 ± 5	89 ± 8	3 ± 1

show that the scattering at this q-range is mainly due to intraparticle form factor correlations (eq 1). The curve of 0.5 mg/mL is divided by 0.55 instead of 0.5 to have perfect agreement. Also we can exclude the possibility of cluster formation from our system which would result in scattering from fractal aggregates[25,26] and would affect $S(q)$ at low q. This is because we do not need to incorporate any such effect in our models to fit the data.

Light Scattering. In Figure 7 we present dynamic light scattering results. The relaxation rate Γ is collected as the position of the maximum of the distribution function of relaxation rate that we obtain from CONTIN analysis of the field autocorrelation functions (inset of Figure 7). As the main relaxation rate (Figure 7) is proportional to q^2, diffusive motion of the scattering centers is observed and the hydrodynamic radius is extracted. There is apparently no concentration dependence of the hydrodynamic radius because the plots of Figure 7 do not show any change for different concentrations. This supports the assumption that our nanoparticles do not interact strongly with each other (dilute solution properties). The values of R_g and M_w are obtained from Zimm plots from the static light scattering data. The aggregation number is calculated from $N_{agg}^{SLS} = M_w/M_{PS\text{-}PSCI}$. There is no evidence of cluster formation since this would appear as a slow mode in the distribution function. In the inset of Figure 7 there is only one dominant dynamical mode. Light scattering results for R_g, R_h and N_{agg} are given in Table 2 for comparison.

Discussion

The size of the PS-core (table 1) is the same under different solution conditions. An increase in the ionic strength or a decrease in the degree of dissociation of chargeable groups on the chains would result in a decrease in the range or intensity of the electrostatic interactions between chain segments. This would favor the aggregation of more chains on the nanoparticles.

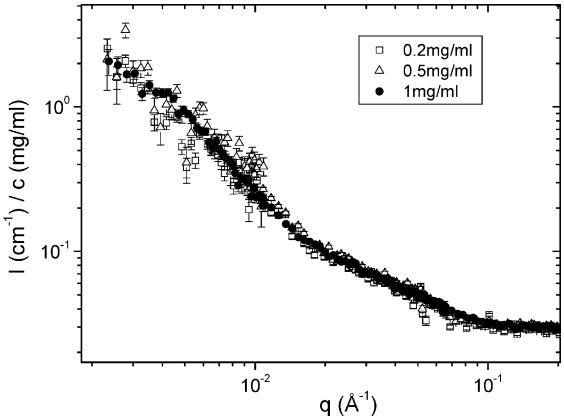

Figure 6. SANS scattered intensity normalized by concentration of PS-PSCI nanoparticles at pH 7 for different concentrations, i.e. 1 mg/mL (filled circles), 0.5 mg/mL (open triangles) and 0.2 mg/mL (open squares).

In the case of polyelectrolyte micelles in equilibrium this would increase the size of the core. In the current study this is not the case because our nanoparticles have PS in their core, which at room temperature is in the glassy state. So they are out of equilibrium "frozen" particles and the PS-core is virtually insensitive to the solution pH and salt content with a stable aggregation number around 4 (Table 1). Additionally, as observed in other investigations, the PS-core and nanoparticle characteristics depend on the preparation protocol.[16,17]

The dense PSCI shell around the PS core is a thin region 1.1 nm in thickness with a volume fraction ~80% (Tables 1 and 2). It has been predicted theoretically[27] that for polyelectrolyte brushes in poor solvents a two-phase brush is induced by attractive binary interactions. Additionally[28] a quasi-neutral regime is predicted for annealed star polyelectrolytes near the center of the star since at this area the steric interactions (nonelectrostatic) dominate over the electrostatic ones. Since in here we have a hydrophobic backbone and some nonfunctionalized hydrophobic isoprene segments in the PSCI chains, we believe that a collapsed layer of PSCI near the core is probable.

A two-region power-law model for the corona layer has been predicted theoretically[28] and also used to model small angle scattering experiments.[29] The power-law $\phi(r) \sim r^{-2}$ is predicted for the so-called osmotic regime where the osmotic pressure of counterions dominates the interactions and the chains are uniformly stretched. Power laws stronger than -2 can be found for annealed polyelectrolyte stars at their periphery.[28] A scaling behavior $\phi(r) \sim r^{-8/3}$ takes into account the gradient in the dissociation ratio of the chains and describes the osmotic annealing regime. Our findings (Table 1) suggest that the PSCI corona consists of an inner layer where the chains are uniformly stretched ($\phi(r) \sim r^{-(1.8\pm0.2)}$) and an outer one where extension because of the gradient in ionization ($\phi(r) \sim r^{-(3.0\pm0.5)}$) occurs. It is predicted by numerical self-consistent model[28] that the gradient in ionization is steeper at the periphery of the nanoparticle than the interior, because of the higher concentration of polymer chains at the interior. Since the scaling of the corona profile (exponents a and b) does not change upon addition of salt (or pH variation), we conclude that the nanoparticles under study are in the osmotic brush regime under all conditions.

For annealed polyelectrolyte micelles the dissociation of groups depends on the pH value or equivalently on the H^+ concentration in solution. The distribution of H^+ in the micellar corona is not uniform as in the bulk solution and is coupled to the local polymer concentration $\phi(r)$. In this way the degree of charging (a) of weak groups is a function of the distance from the center, i.e. $a = a(r)$. A unique property of annealed polyelectrolyte brushes is the nonmonotonous changes of their size as a function of salt content. At low salt content salt ions are exchanged with the H^+ ions, and this shifts the dissociation equilibrium to higher charging ratios. So the electrostatic interactions become stronger and the chains extend further. As

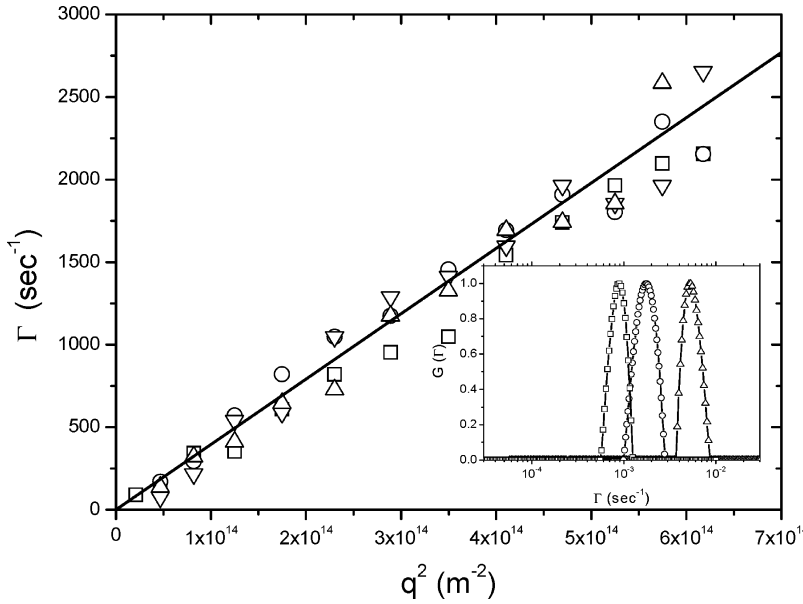

Figure 7. Relaxation rate Γ extracted by CONTIN analysis as a function of q^2 for PS-PSCI nanoparticles at pH 7 for several polymer concentrations, i.e. 1 mg/mL (squares), 0.5 mg/mL (circles), 0.2 mg/mL (down triangles) and 0.1 mg/mL (up triangles). The straight line highlights the proportionality between Γ and q^2. Inset: CONTIN analysis of correlation functions collected at 30° (up triangles), 60° (circles) and 90° (squares) for 1 mg/mL PS-PSCI at pH 7 with no added salt.

the salt content increases more, the charge screening dominates and the brush starts to shrink.

We observe a possible decrease of R_{int} between 28 ± 2, to 27 ± 2 and to 24 ± 2 nm for no added salt, 0.1 and 0.5 M added salt respectively (Table 2). Also the total size R_M of the nanoparticles shows a trend to decrease upon addition of salt, from 82 ± 5, 78 ± 5 and 75 ± 5 nm. Although the values above give evidence for systematic decrease upon addition of salt, their change is within the limits of the "resolution" of our fitting procedure. This small decrease could be explained by the onset of screening of electrostatic interactions.

Furthermore, increasing the pH of the solution from 3 to 7 and finally to 9 there is no evidence of change of R_{int} (28 ± 2 nm) but an increase in R_M (71 ± 2 nm, 82 ± 5, 86 ± 5 nm) is observed (Table 2). The outer corona is indeed the regime which should be strongly influenced by pH changes because this regime is dominated by ionization gradient effects. The degree of ionization of the COO^- acidic group is expected to increase with pH, and this enhances the electrostatic repulsions, i.e. increases the layer size.

The maximum length scale of the nanoparticle SANS form factor is R_M and is normally compared to the hydrodynamic radius R_h as obtained by DLS. As seen in Table 2, R_M is generally higher than R_h, and one explanation for this could be penetration of the solvent in the outer periphery of the starlike nanoparticle. For pH 7 with no added salt and pH 9 with no added salt R_h and R_M agree within experimental error. These are the cases where R_g from SANS and R_g from SLS agree as well. In the other three solution conditions (Table 2) R_g from SANS appears lower than R_g from SLS, and this is possibly because of the different kinds of contrasts observed by the two techniques. Finally, the aggregation number N_{agg} measured by SLS appears to be in the range of the one found by SANS (4.1 ± 0.3). We believe that the SANS method is more robust for the determination of N_{agg} in this investigation because N_{agg}^{SANS} is defined by the size of the PS-core, which is fairly independent from the choice of volume fraction profile model. The SLS contrast factor $K = [4\pi^2 n_0^2/(\lambda^4 N_A)](dn/dc)^2$ depends on the refractive index increment dn/dc of the polymer with respect to the solvent. In our Zimm analysis we have used the same dn/dc value for all solution conditions which was calculated as a weight average of the dn/dc of the two blocks of the diblock polymer chains in pure water. This assumption could not be accurate since our solvent contrast may change by the addition of ions (introduced in order to set the pH and salt content) and may result in a virtual variation of the molecular weight.

Conclusions

The analysis of the scattering from PS-PSCI block polyelectrolyte nanoparticles was presented. The SANS data were modeled by spherical form factors with radial dependence of the volume fraction. A spherical compact PS-core surrounded by a charged PSCI corona is the coarse structure of the particles. The charged corona consists of an inner layer where the volume fraction scales as $\phi(r) \sim r^{-(1.8\pm0.2)}$ and an outer layer with $\phi(r) \sim r^{-(3.0\pm0.5)}$. These exponents are near the ones predicted theoretically by Borisov et al.[5] as the osmotic brush regime $\phi(r) \sim r^{-2}$ and the annealing osmotic brush regime $\phi(r) \sim r^{-8/3}$. In order for the number of blocks inside the PS-core to be equal to the number of blocks in the corona, we introduce a concentrated shell of collapsed segments of PSCI next to the PS-core. This shell is possible to exist since at distances near the center the concentration of monomers and counterions is high so that the steric interactions (hydrophobic in this case) dominate the electrostatic ones. The size of the nanoparticles tends to decrease as the salt content increases due to the screening of the electrostatic interactions. On the other hand the outer layer of the spherical brushes swells by increasing the pH because of the expected increase in the degree of ionization.

Acknowledgment. The SANS experiments have been supported by the European Commission under the seventh Framework Programme through the Key Action: Strengthening the European Research Area, Research Infrastructures. Contract No.: 226507 (NMI3). The SANS work is based on experiments performed at the Jülich Centre for Neutron Science JCNS, Forschungszentrum Jülich, Germany.

References and Notes

(1) Harada, A.; Kataoka, K. Supramolecular assemblies of block copolymers in aqueous media as nanocontainers relevant to biological applications. *Prog. Polym. Sci.* **2006**, *31*, 949–982.

(2) Forster, S.; Abetz, V. A.; Muller, H. E. Polyelectrolyte Block Copolymer Micelles. *Adv. Polym. Sci.* **2004**, *166*, 173–210.

(3) Ruhe, J.; Ballauff, M.; Biesalski, M.; Dziezok, P.; Grohn, F.; Johannsmann, D. Polyelectrolyte Brushes. *Adv. Polym. Sci.* **2004**, *165*, 79–150.

(4) Ballauff, M. Spherical polyelectrolyte brushes. *Prog. Polym. Sci.* **2007**, *32*, 1135–1151.

(5) Borisov, O. V.; Zhulina, E. B. Effects of ionic strength and charge annealing in star-branched polyelectrolytes. *Eur. Phys. J. B* **1998**, *4*, 205–217.

(6) Guenoun, P.; Muller, F.; Delsanti, M.; Auvray, L.; Chen, Y. J.; Mays, J. W.; Tirrell, M. Rodlike Behavior of Polyelectrolyte Brushes. *Phys. Rev. Lett.* **1998**, *81*, 3872–3875.

(7) Pincus, P. Colloid Stabilization with Grafted Polyelectrolytes. *Macromolecules* **1991**, *24*, 2912–2919.

(8) Alexander, S. Adsorption of chain molecules with a polar head: a scaling description. *J. Phys. (Paris)* **1977**, *38*, 983.

(9) Daoud, M.; Cotton, J. P. Star shaped polymers: a model for the conformation and its concentration dependence. *J. Phys. (Paris)* **1982**, *43*, 531–538.

(10) Papagiannopoulos, A.; Fernyhough, C. M.; Waigh, T. A. The microrheology of polystyrene sulfonate combs in aqueous solution. *J. Chem. Phys.* **2005**, *123*, 214904.

(11) Papagiannopoulos, A.; Fernyhough, C. M.; Waigh, T. A.; Radulescu, A. Scattering Study of the Structure of Polystyrene Sulfonate Comb Polyelectrolytes in Solution. *Macromol. Chem. Phys.* **2008**, *209*, 2475–2486.

(12) Papagiannopoulos, A.; Waigh, T. A.; Hardingham, T.; Heinrich, M. Solution Structure and Dynamics of Cartilage Aggrecan. *Biomacromolecules* **2006**, *7*, 2162–2172.

(13) Higgins, J. S.; Benoit, H. C. *Polymers and Neutron Scattering*; Oxford University Press: New York, 1994.

(14) Pedersen, J. S.; Svaneborg, C. Scattering from block copolymer micelles. *Curr. Opin. Colloid Interface Sci.* **2002**, *7*, 158–166.

(15) Pispas, S. Complexes of Lysozyme with Sodium (Sulfamate-Carboxylate)Isoprene/Ethylene Oxide Double Hydrophilic Block Copolymers. *J. Polym. Sci., Part A: Polym. Chem.* **2007**, *45*, 509–520.

(16) Mountrichas, G.; Pispas, S.; Tagmatarchis, N. Aqueous Carbon-Nanotube-Amphiphilic-Block-Copolymer Nanoensembles: Towards Realization of Charge-Transfer Processes with Semiconductor Quantum Dots. *Small,* **2007**, *3*, 404–407.

(17) Uchman, M.; Prochazka, M.; Stepanek, M.; Mountrichas, G.; Pispas, S.; Spirkova, M.; Walther, A. pH-Dependent Self-Assembly of Polystyrene-block-Poly((sulfamate-carboxylate)isoprene) Copolymer in Aqueous Media. *Langmuir* **2008**, *24*, 12017–12025.

(18) Pispas, S. Double Hydrophilic Block Copolymers of Sodium(2-sulfamate-3-carboxylate)isoprene and Ethylene Oxide. *J. Polym. Sci., Part A: Polym. Chem.* **2006**, *44*, 606–613.

(19) Barker, J. G.; Pedersen, J. S. Instrumental Smearing Effects in Radially Symmetric Small-Angle Neutron Scattering by Numerical and Analytical Methods. *J. Appl. Crystallogr.* **1995**, *28*, 105–114.

(20) Pedersen, J. S. Analysis of small-angle scattering data from colloids and polymer solutions: modeling and least-squares fitting. *Adv. Colloid Interface Sci.* **1997**, *70*, 171–210.

(21) Schmidt, V.; Di Cola, E.; Giacomelli, C.; Brisson, A. R.; Narayanan, T.; R., B. Polyelectrolyte Behavior of Diblock Copolymer Micelles Having Phosphonic Diacid Groups at the Corona. *Macromolecules* **2008**, *41* (6), 2195–2202.

(22) Forster, S.; Hermsdorf, N.; Bottcher, C.; Lindner, P. Structure of Polyelectrolyte Block Copolymer Micelles. *Macromolecules* **2002**, *35*, 4096–4105.

(23) Forster, S.; Wenz, E.; Lindner, P. Density Profile of Spherical Polymer Brushes. *Phys. Rev. Lett.* **1996**, *77*, 95–98.

(24) Waigh, T. A.; Papagiannopoulos, A.; Voice, A.; Bansil, R.; Unwin, A. P.; Dewhurst, C. D.; Turner, B.; Afdhalr, N. Entanglement Coupling in Porcine Stomach Mucin. *Langmuir* **2002**, *18*, 7188–7195.

(25) Teixera, J. Small-angle scattering by fractal systems. *J. Appl. Crystallogr.* **1988**, *21*, 781–785.

(26) Beaucage, G. Small-Angle Scattering from Polymeric Mass Fractals of Arbitrary Mass-Fractal Dimension. *J. Appl. Crystallogr.* **1996**, *29*, 134–146.

(27) Misra, S.; Mattice, W. L.; Napped, D. H. Structure of Polyelectrolyte Stars and Convex Polyelectrolyte Brushes. *Macromolecules* **1994**, *27*, 7090–7098.

(28) Wolterink, J. K.; Van Male, J.; Cohen Stuart, M. A.; Koopal, L. K.; Zhulina, E. B.; Borisov, O. V. Annealed Star-Branched Polyelectrolytes in Solution. *Macromolecules* **2002**, *35*, 9176–9190.

(29) Van Der Maarel, J. R. C.; Groenewegen, W.; Egelhaaf, S. U.; Lapp, A. Salt induced concentration of polyelectrolyte diblock copolymer micelles. *Langmuir* **2000**, *16*, 7510–7519.

JP1009912